The systematic study of the precursor ratios effect in the Cd-Zn-S quantum dots synthesis

Liudmila Loghina[a*], Anastasia Kaderavkova[a], Maksym Chylii[a], Bozena Frumarova[a], Petr Svec[b], Stanislav Slang[a] and Miroslav Vlcek[a]

[a]*Center of Materials and Nanotechnologies, Faculty of Chemical Technology, University of Pardubice, nam. Cs. legii 565, Pardubice 530 02, Czech Republic*
[b]*Department of General and Inorganic Chemistry, Faculty of Chemical Technology, University of Pardubice, Studentska 95, Pardubice 532 10, Czech Republic*

[*] The corresponding author's e-mail: Liudmila.Loghina@upce.cz

Abstract

Semiconductor Quantum Dots (QDs) have attracted a great attention due to their unique optical and chemical properties. An increasing demand for size- and shape uniformity of QDs, high quantum yield (QY) and photochemical stability can be resolved by synthetic methods. Here we report a study of the effect of the precursors' ratios within the synthesis of the Cd-Zn-S QDs series. The trisubstituted thiourea (N-phenylmorpholine-4-carbothioamide) as a new and environmentally friendly source of sulphur in the synthesis of $Cd_{0.2}Zn_{0.8}S$ QDs (Cd, Zn : S molar ratios = 1 : 0.5; 1 : 1; 1 : 1.5; 1 : 2; 1 : 2.5) and $Cd_xZn_{1-x}S$ QDs (where x = 0.1; 0.25; 0.5; 0.75; 0.9) has been investigated. It was determined that an increase in the molar ratio of trisubstituted thiourea to metals leads to the growth of QDs, and, as a consequence, to a small emission's red shift in the visible region of the spectrum. However, no significant changes in the elemental ratio in the material were detected. It was found that with an excess of trisubstituted thiourea taken to the reaction, oleylamine (OAm) as a *co*-ligand replaces linoleic acid from the protective shell of QDs. In the case of an increase of Cd content in the $Cd_xZn_{1-x}S$ QDs, a significant shift in the emission to the red region of the spectrum was observed with an increase in the size of the QDs and while their shape was unchanged. Based on the XRD data, a gradual transition from a cubic to a hexagonal crystal structure was detected. The high quantum yield (70 %), narrow photoluminescence (PL) signal (FWHM < 31 nm) and the size uniformity of the obtained nanomaterials are promising features for high-sensitive sensors and LEDs production.

Keywords: synthesis, quantum dots, substituted thioureas,

1. Introduction

Extensive research in the field of nanomaterials' synthesis is caused by the growing demand from both academy and industry. A significant place is taken by semiconductor QDs with binary and multicomponent compositions. Such QDs have found various applications in the development and manufacture of light-emitting diodes (LEDs) [1-3], sensitive markers introduced into living organisms [4-6], photovoltaic devices [7], alpha, gamma, and neutron scintillators [8-12] for medical purposes and space research. Moreover, the successful implementation of chalcogenide QDs in the creation of solar cells [13,14] and catalysts for reaction processes [15-17] have been reported. Certainly, such a variety of QDs' applications is caused by their unique properties,

which are directly dependent on the chemical composition and QDs' shapes and sizes. Now, there are many synthetic approaches to the production of QDs and each of them leads to the formation of nanomaterials with definite properties. Considering the approaches to the synthesis of Cd-Zn-S QDs, one should highlight some recent developments.

Core/shell ZnCdS/ZnS and ZnCdS/$Cd_xZn_{1-x}S$/ZnS QDs were successfully integrated into the hybrid QD-based light-emitting device structure as the emissive layer [18]. According to O. Wang *et al*., the covering of a QD with a shell of a ternary $Cd_xZn_{1-x}S$ composition can significantly increase not only the quantum yield (PL QY up to 100 %) but also the external quantum (up to 18 %) and current efficiencies. The ternary ZnCdS QDs were synthesized using air-stable compounds by facile and low-cost aqueous synthetic method [19]. The authors demonstrated the influence of the reaction process conditions on the properties of ZnCdS QDs with various Cd/Zn ratios. White light-emitting CdS core and $Cd_xZn_{1-x}S$ shell QDs (the quantum efficiency up to 34 %) have been synthesized based on the corresponding acetates and sulphur dissolved in 1-octadecene (ODE) as a single step non-injection technique [20].

The design of any nanostructure preparation comprises many aspects, including the safety of synthesis while achieving of the necessary physical and chemical characteristics of nanomaterials. Various factors influence the production of nanomaterials with the desired properties. A protective shell consisting of one or more ligands plays an important role both in the formation of the nanocrystal and in the determination of the chemical and physical properties of the final product [21]. The main purpose of the protective shell is to prevent the agglomeration of QDs, and to transfer the QDs to an organic or inorganic medium in the form of a sol [22]. Currently, the most effective agents for the formation of a protective shell are fatty carboxylic acids [23]. The presence of a double bond in a carboxylic acid molecule increases the "solubility" of QDs in low-polar organic media. Also, higher thiols [24] and amines [25] are considered as effective ligands. Moreover, the nature of the solvent affects the formation (nucleation and growth) of QDs. The solvent's ability to coordinate molecules, as well as the ability of solvation of QDs, i.e. the ligand affinity to form a protective shell, provides a level of saturation in the system and uniform crystal growth [26]. In summary of the foregoing, oleic (OA) or linoleic (LA) acid with 1-octadecene (ODE) can be considered as a convincing combination for the synthesis of QDs. Up to date, sulphur dissolved in ODE [27,28] and trialkylphosphine sulphides [29,30] are the most common sulphur sources in the synthesis of chalcogenide QDs. Each of these agents has its advantages and disadvantages in terms of production.

A multicomponent quantum dot, consisting of a wide band gap (zinc chalcogenides) and medium band gap (cadmium chalcogenides) semiconductors, forms an alloy with a different mutual distribution of the materials, which in turn leads to a modification of the energy spectrum. The mutual "solubility" of semiconductors depends on their formation rate, which is also influenced by the nature of the sulphur source.

In this paper, we present the synthesis of highly photoluminescent Cd-Zn-S QDs using an available, environmentally friendly, and at the same time highly reactive sulphur source. N-phenylmorpholine-4-carbothioamide was prepared by condensation of phenyl isothiocyanate with morpholine in a quantitative yield. We studied the influence of the deficiency and excess of the sulphur precursor taken to the synthesis of $Cd_{0.2}Zn_{0.8}S$ QDs in comparison with its equimolar ratio to metals. It was found that a significant excess of the trisubstituted thiourea introduced

into the reaction leads to a replacement of the ligand forming the protective shell of the QDs. As an additional contribution to the development of the proposed method, the influence of N-phenylmorpholine-4-carbothioamide as a new sulphur source on the structure and optical properties of $Cd_xZn_{1-x}S$ QDs (x = 0.1; 0.25; 0.5; 0.75; 0.9) prepared with equimolar cation-anion ratios is presented. Synthesized QDs possess a high PL QY up to 70 % and high colour purity (FWHM < 31 nm). The average PL lifetime of band edge emission and trap state emission of ternary Cd-Zn-S QDs are in the range of ∼0.01 - 12 ns and ∼17 - 115 ns, respectively, depending on metals and sulphur precursors ratios.

2. Experimental section

2.1 Materials

Cadmium oxide (CdO, 99.99 %), zinc oxide (ZnO, 99 %), oleylamine (OAm, technical grade, 70 %), linoleic acid (LA, technical grade, 60-74 %), 1-octadecene (ODE, technical grade, 90 %), phenyl isothiocyanate (98 %), morpholine (99 %), chloroform-d ($CDCl_3$, 99.8 atom % D) were purchased from Sigma-Aldrich. Solvents used for the purification of organic precursors and prepared QDs were purchased from Fisher Scientific. Syntheses of QDs were carried out using standard Schlenk techniques under an Ar atmosphere.

2.2 Synthesis of $Cd_{0.2}Zn_{0.8}S$ QDs with different Cd, Zn : S precursors ratios

The influence of the deficiency or excess of trisubstituted thiourea to a mixture of metals was studied under the constant conditions (temperature, the concentration of the starting components, *etc*.). The only variable factor was the molar ratios of Cd, Zn : S precursors (1 : 0.5; 1 : 1; 1 : 1.5; 1 : 2; 1 : 2.5). The proposed synthetic procedure for the preparation of $Cd_{0.2}Zn_{0.8}S$ QDs consists of three parts: synthesis of N-phenylmorpholine-4-carbothioamide (**TU**) as a source of sulphur and its transfer to a solution of OAm and ODE, synthesis of metal linoleates (as sources of cadmium and zinc) and synthesis QDs by hot-injection technique at 280 °C. All the steps are described in detail below.

*2.2.1 Synthesis of N-phenylmorpholine-4-carbothioamide (**TU**)*

Phenyl isothiocyanate (PhNCS, 6.76 g, 0.05 mol) and 100 ml of toluene were placed in a 250 ml round bottom flask. Morpholine (4.36 g, 0.05 mol) was added in portions (exothermic reaction) to the same flask under stirring at room temperature. Further, the reaction mixture was stirred for 2 hours at room temperature. The precipitated **TU** was filtered off and washed with cold toluene providing pure **TU** which was dried in the air.

White solid, isolated yield 10.45 g (94 %). FT-IR (single-bounce diamond ATR crystal, cm^{-1}): ν(NH) 3230, ν(CH) 2915, ν(Ar) 1661, ν(C=S) 1241. ^{1}H NMR (400.13 MHz, $CDCl_3$): 7.52 (s, 1H, NH), 7.32 (t, 2H, *J* = 7.8 Hz, H^{arom}), 7.15 (t, 1H, *J* = 7.4 Hz, H^{arom}), 7.11 – 7.13 (d, 2H, *J* = 7.77, H^{arom}), 3.76 – 3.78 (m, 4H, CH_2-O-CH_2), 3.67 – 3.69 (m, 4H, CH_2-N-CH_2). ^{13}C NMR (100.61 MHz, $CDCl_3$): 183.6 (C=S), 140.0 (C^{arom}), 129.3 (C^{arom}), 125.5 (C^{arom}), 123.4 (C^{arom}), 66.2 (CH_2-O-CH_2), 49.7 (CH_2-N-CH_2).

For the further use in the synthesis, trisubstituted thiourea was dissolved in a mixture of ODE and OAm at 40 - 50 °C. The amount of OAm was 1.5 molar equivalents of selected **TU** so that the injected solutions have approximately the same volume.

2.2.2 Synthesis of metal linoleates

CdO (0.154 g, 0.0012 mol), ZnO (0.391 g, 0.048 mol), linoleic acid (LA, 5.05 g, 0.018 mol) and 10 ml ODE were placed in a 50 ml Schlenk flask. The mixture was degassed upon vigorous stirring according to the following scheme: for 10 minutes at room temperature, then for 20 minutes at 100 °C and then with an increase of temperature up to 200 °C. By replacing the air (together with the evolving water vapor) by argon, the reaction mixture was heated up to 280 °C (operating temperature) and stirred in argon until the mixture was completely homogenized. Complete homogenization indicates the final conversion of metal oxides to the corresponding linoleates. The resulting solution was used as a matrix for introducing a sulfur precursor.

2.2.3 Synthesis of $Cd_{0.2}Zn_{0.8}S$ QDs (different ratios of Cd, Zn : S precursors)

A freshly prepared solution of trisubstituted thiourea was added in one portion to a solution of metal linoleates under constant stirring at 280 °C under the low Ar flow. For each synthesis, aliquots were taken at certain intervals from the moment of the sulfur precursor's injection. This step was necessary to evaluate the nucleation and growth of QDs. 30 µl of each aliquot were dissolved in 2 ml of $CHCl_3$ and then their absorbance (ABS) and photoluminescence (PL) spectra were measured. The duration of the synthesis was 20 minutes. Afterwards, the reaction mixture was allowed to cool spontaneously to about 50 °C and a "cold" aliquot was taken. Its measured ABS and PL spectra were added to the QDs growth overview. The cooled reaction mixture was transferred to 30 ml of $CHCl_3$ and QDs were precipitated with a mixture of acetone and methanol (10 : 1). The precipitated nanocrystals were separated by centrifugation, then further purified through re-dissolution in $CHCl_3$ and subsequent precipitation. The purification process was repeated twice more to achieve a complete removal of by-products and all starting compounds. QDs were dried *in vacuo* at room temperature for 4 hours. The isolated yield of $Cd_{0.2}Zn_{0.8}S$ QDs was 0.6 - 0.7 g.

2.3 Synthesis of $Cd_xZn_{1-x}S$ QDs (different ratios of metal precursors)

The synthesis of $Cd_xZn_{1-x}S$ QDs was carried out using various metal ratios. For the series of syntheses we selected the following Cd : Zn ratios: 0.1 : 0.9; 0.25 : 0.75; 0.5 : 0.5; 0.75 : 0.25; 0.9 : 0.1. The syntheses of metal linoleates in ODE were conducted according to the method described above only by changing the metals ratios. The same trisubstituted thiourea, which was used for the preparation of the previous series, was taken in 1 : 1 molar ratio to Cd and Zn metals. A freshly prepared solution of N-phenylmorpholine-4-carbothioamide (**TU**, 1.33 g, 0.006 mol) in 2.4 g OAm and 1.6 g ODE was injected in one portion to a solution of metal linoleates at 280 °C with constant stirring under Ar. The total growth time of QDs (from the moment of sulfur precursor's injection) was 20 minutes. The monitoring of each synthesis was carried out by taking aliquots from the reaction mixture at regular intervals and then measuring ABS and PL spectra. Isolation and purification of QDs were similar to described above. The isolated yield of QDs was 0.6 - 0.8 g.

2.4 Characterization

The Nuclear Magnetic Resonance (NMR) spectra were recorded from solutions in $CDCl_3$ at 295 K on a Bruker 400 UltraShieldTM spectrometer (equipped with a Z-gradient 5 mm BBO probe at frequencies 400.13 MHz for ^1H and 100.61 MHz for ^{13}C $\{^1H\}$). The solutions were obtained by dissolving approximately 50 mg of each compound in 0.6 ml of $CDCl_3$. The values of ^1H chemical shifts were calibrated to residual signals of $CDCl_3$ (δ (^1H) = 7.26 ppm). The values of ^{13}C chemical shifts are referred to signals of $CDCl_3$ (δ (^{13}C) = 77.23 ppm). Positive chemical shift values denote shifts to the higher frequencies relative to the standards.

IR spectra in the region 4000 - 50 cm^{-1} (resolution 2 cm^{-1}) were recorded on Vertex 70v FT-IR spectrometer (Bruker, Germany) using single-bounce diamond ATR crystal. X-Ray diffraction patterns (XRD) were registered using PANalytical EMPYREAN powder X-Ray diffractometer (ALMELO, Netherlands) with Cu-Kα radiation (λ = 1.5418 Å). Data were obtained across a 2θ range of 20 - 70° with a step size of 0.05°. Energy dispersive X-Ray (EDX/EDS) spectroscopy was performed also to analyse the chemical composition of QDs using scanning electron microscope LYRA 3 (Tescan, Czech Republic) equipped with EDX detector AZtec X-Max 20 (Oxford Instruments, UK) at 20 kV acceleration voltage. The same device was used for STEM measurements using retractable STEM detector (Tescan, Czech Republic) at 30 kV acceleration voltage.

The chemical composition of Cd-Zn-S QDs was determined by X-Ray photoelectron spectroscopy (XPS, ESCA 2SR, Scienta-Omicron) by monochromatic Al Kα source (1486.6 eV). Nanopowders were pressed into C tape for the XPS. The binding energy scale was referenced to adventitious carbon (284.8 eV) and the quantitative analysis was carried out using sensitivity factors provided by the manufacturer.

The optical properties measurements of all synthesized Cd-Zn-S QDs were performed on Fluorometer PTI QuantaMaster 400 (Horiba, Germany) to obtain PL data in spectral range 250 - 800 nm using excitation wavelength λ = 300 - 400 nm and UV-3600 (Shimadzu, Japan) spectrometer to get UV-VIS absorbance spectra in the spectral range 200 - 800 nm. The PL lifetime measurements were performed using TCSPC accessories for Fluorometer PTI QuantaMaster 400 with 362 nm and 391 nm light pulse excitation and the pulse half-width 0.8 ns produced by NanoLED-360 and NanoLED-390 LEDs respectively (Horiba Scientific). Photoluminescence decay kinetics curves were analysed by PTI Felix GX software.

3. Results and discussion

3.1 Synthesis of Cd-Zn-S QDs

Earlier, we presented the mechanism of interaction between cadmium and zinc linoleates and substituted thiourea [31]. Our findings demonstrate that the reaction proceeds via the formation of a substituted thiourea's complex with metal carboxylates and its further decomposition to the corresponding sulphides with a partial release of hydrogen sulphide. As reported, at the moment of QDs growth, there is a certain lack of sulphur ions and an excess of metal carboxylates due to which the protective shell of the QDs is formed. In the case of using equivalent cation-anion

ratios, several studies were conducted with the involvement of various di- and trisubstituted thioureas [32]. However, the question of the effect of substituted thioureas on the structure and optical characteristics of QDs in non-equivalent ratios of the starting components remains open.

To answer this question, a series of experiments were carried out using different ratios of Cd, Zn : S precursors (1 : 0.5; 1 : 1; 1 : 1.5; 1 : 2; 1 : 2.5). Thus, $Cd_{0.2}Zn_{0.8}S$ QDs were synthesized with a deficiency, an equal ratio, and an excess of trisubstituted thiourea to metal carboxylates employed in the reaction. The synthetic scheme is presented in **Figure 1**. Therefore, metal linoleates obtained from the corresponding oxides interact with trisubstituted thiourea to form sulphides. The reaction proceeds through the formation of an intermediate complex with its further decomposition to a mixed sulphide.

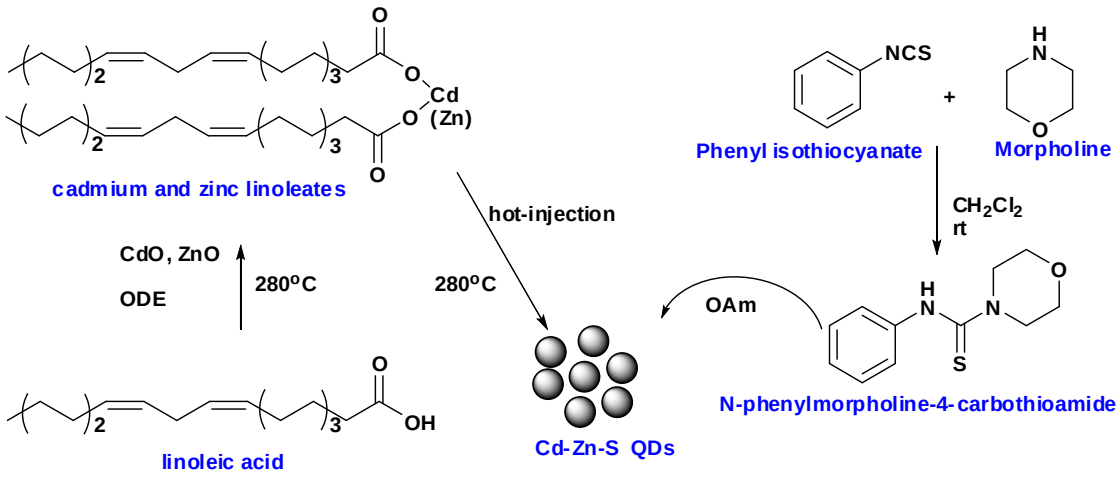

Figure 1. Overview of Cd-Zn-S QDs preparation.

The distribution of elements in the quantum dot is determined by several factors, among which the most considerable are the formation and subsequent decomposition rates of complexes to sulphides. In the case of the use of substituted thioureas, these rates are close to each other, in particular for cadmium and zinc, with a nearly homogeneous distribution of cations in the QDs. To study the effect of trisubstituted thiourea on the rate of formation and decomposition of complexes, various Cd : Zn ratios (0.1 : 0.9; 0.25 : 0.75; 0.5 : 0.5; 0.75 : 0.25; 0.9 : 0.1) were taken. Keeping all the other reaction conditions constant, including the equivalent cation-anion ratio, only the metal ratios were changed.

3.2 Mechanism of QD's formation

Starting from the moment of nucleation, free metal carboxylates and their complexes with trisubstituted thiourea coexist in the reaction mixture. Following the decomposition of the intermediate complex, the equilibrium shifts toward the formation of sulphides, which concentration increases rapidly. OAm, which is present in the growth medium of nanocrystals as a *co*-ligand, participates in the parallel formation of amide, removing carboxylate residues from the medium. Thus, OAm also contributes to a shift in equilibrium towards sulphide's formation. When the saturation of the colloidal solution is achieved, crystal growth begins, thereby removing excess of molecular sulphides from the system. Since all these processes occur simultaneously, metal linoleates, free linoleic acid, and complexed trisubstituted thiourea are constantly present in the medium. Over time, the concentration of the starting and intermediate

components decreases, and the crystal growth process slows down. The role of metal carboxylates in the formation of a nanocrystal is determined not only by their interaction with trisubstituted thiourea but also by the formation of a protective shell that prevents particles from aggregation. This shell exists due to some excess of carboxylates in the reaction medium. However, in the case of a twofold or more excess of trisubstituted thiourea in the system, the equilibrium is completely shifted towards the formation of sulphides, involving all molecules of metal carboxylates to the reaction. In this case, OAm is acting as a *co*-ligand and becomes the dominant ligand that forms the protective shell of QDs. This sequential ligand replacement was confirmed by FT-IR spectra (see *FT-IR spectral studies of Cd-Zn-S QDs*).

In addition, the growth process of QDs can be estimated by measuring the optical properties of aliquots taken during the reaction process. Changes in the absorbance (ABS) and photoluminescence (PL) spectra of growing QDs are illustrated in **Figure 2**. Samples taken from the reaction mixture during QD's growth (10 sec, 20 sec, 60 sec, 120 sec, 300 sec, 600 sec and 1200 sec) were taken as 30 µl aliquots. It can be noticed that from the first seconds of trisubstituted thiourea's injection, a PL signal and its corresponding exciton appear in the PL and ABS spectrum respectively.

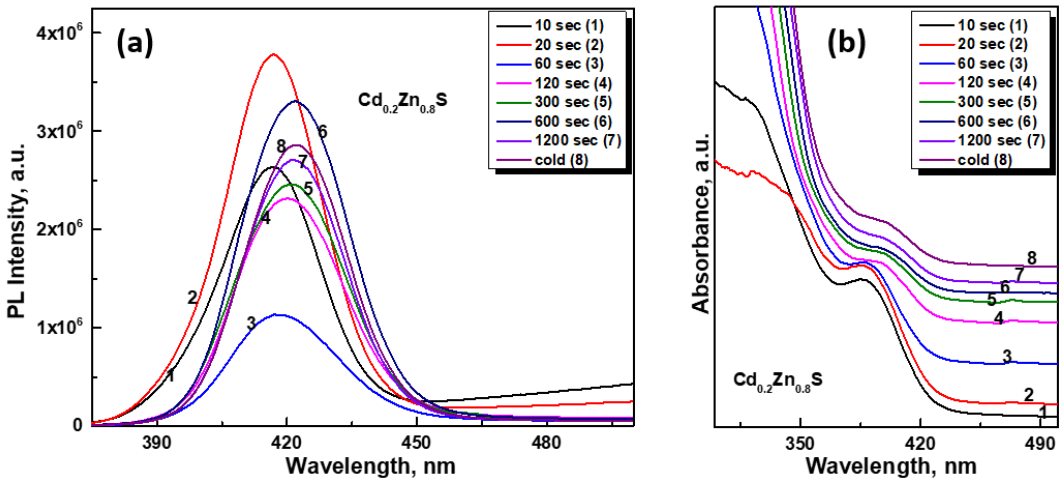

Figure 2. Photoluminescence (a) and UV-VIS absorbance spectra (b) of the growth of $Cd_{0.2}Zn_{0.8}S$ QDs prepared with Cd, Zn : S precursor ratio 1 : 1.5.

Further, a certain shift in the wavelength is observed in the PL spectra as well as a change in the intensity of the signal. Such changes indicate a decrease and an increase in the QDs' concentration in the system. In the process of formation and especially intensive growth of QDs during the first seconds after the N-phenylmorpholine-4-carbothioamide´s injection, quantum dots (QDs) with different sizes coexist in the reaction mixture, which leads to a broadening of the photoluminescence signal (**Fig. 2a**) and corresponding changes in the intensity of the first exciton maximum in the absorbance spectra (**Fig. 2b**). According to the phenomenon of the luminescence concentration quenching, the concentration of QDs in taken from reaction mixture aliquots increases, which leads to a decrease of the photoluminescence signal intensity. The concentration of these QDs in the reaction system is constantly changing due to the redistribution of smaller crystals and the ongoing simultaneous interaction of N-phenylmorpholine-4-carbothioamide with metal linoleates.

In our opinion, 60 seconds from the moment N-phenylmorpholine-4-carbothioamide´s injection is a turning point in which the interaction of the starting components ceases, and the equilibrium is completely shifted towards the formation of nanocrystals. After 120 seconds, QDs concentration was stabilized and PL intensity was not changed so drastically. During the next 20 minutes growth of QDs, a small but stable shift to the red region of the spectrum is observed. A similar tendency can be noticed in the first exciton's shift in the ABS spectra. Homogeneity in the signal's width and the same shift in the growth spectra indicates the homogeneity of the nanocrystal, consisting of the three elements. After 20 minutes of QDs' growth at 280 °C, the reaction mixture was allowed to cool spontaneously, after that a "cold" sample was taken. According to the PL and ABS spectra of this probe, the growth of QDs slowed down significantly but did not finish after switching off the heating. The termination of QDs' growth can be achieved only in the case of the removal of all initial components from the system, i.e. during the purification process.

3.3 Structural analysis and morphology of synthesized Cd-Zn-S QDs

3.3.1 FT-IR spectral studies of Cd-Zn-S QDs

The ATR spectra of studied samples are presented in **Figure 3a, b**. Characteristic vibrations of organic units are in the region between 3600 and 400 cm^{-1}, vibrations of inorganic moieties are between 400 and 50 cm^{-1}. All the data were scaled by the maximum intensity of the absorbance band corresponding to vibration modes of inorganic part of QDs. The obtained experimental data indicate the presence of a large aliphatic fragment in the region of 3050 - 2800 cm^{-1}, corresponding to the symmetric and asymmetric stretching vibrations of $-CH_2-$ and CH_3- groups [33-35]. The spectra of oleylamine (**Fig. 3b**) and linoleic acid (**Fig. 3a**) were taken for the comparison to illustrate the presence of these fragments in both molecules.

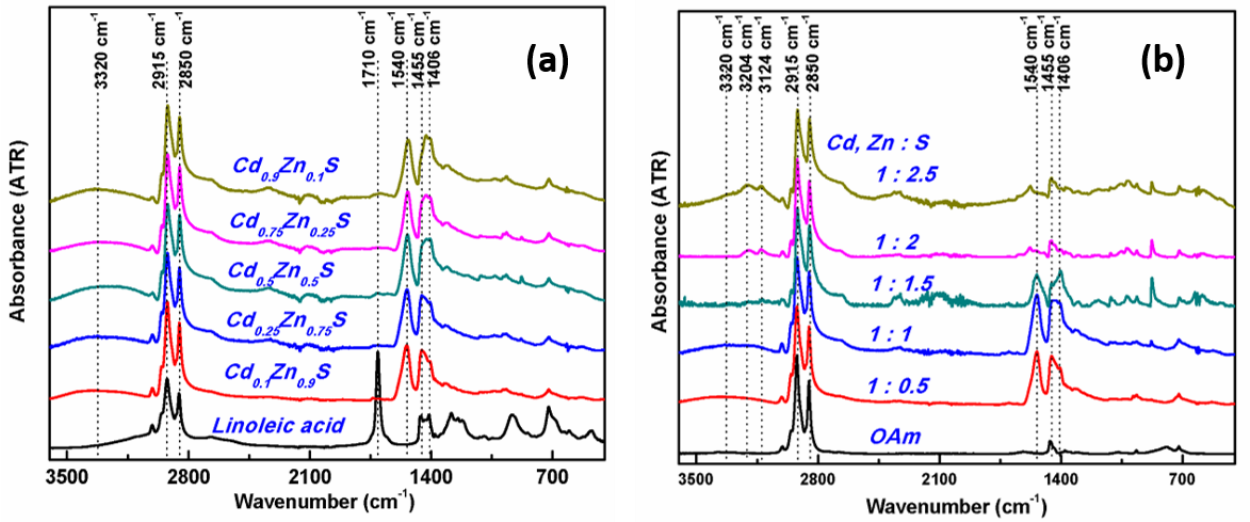

Figure 3. FT-IR spectra of prepared Cd-Zn-S QDs (in comparison with FT-IR spectra of (a) linoleic acid and (b) oleylamine).

It should be noted that there is no signal of the free carboxyl group -COOH at 1710 cm^{-1} for all synthesized Cd-Zn-S QDs but the presence of two characteristic signals between 1695 - 1540 cm^{-1} and 1440 - 1335 cm^{-1} is indicative of the presence of salts of carboxylic acids [33]. The first very strong band is related to COO- asymmetric stretching vibrations (ν_{as}). The second broad band, which is associated with COO- symmetric stretching vibrations (ν_s) generally has two or three peaks [34]. In the case of $Cd_{0.1}Zn_{0.9}S$ QDs (**Fig. 3a**), the band of ν_{as} (COO-) was found at 1540 cm^{-1}. The maximum of this band is slightly shifted to smaller wavenumbers with an increasing amount of Cd^{2+} ions (1530 cm^{-1} for $Cd_{0.9}Zn_{0.1}S$ QDs). The broad band corresponding to ν_s (COO-) vibrations was deconvoluted in region 1480 - 1380 cm^{-1} to 5 peaks with maxima at 1465 cm^{-1}, 1455 cm^{-1} (δ CH_3-, δ CH_2-) and at 1441 cm^{-1}, 1428 cm^{-1} and 1406 cm^{-1} (ν_s COO-). The difference between positions of asymmetric and symmetric stretching vibrations of COO- group ($\Delta = \nu_{as} - \nu_s$) [35-37] in ATR spectra of $Cd_{0.1}Zn_{0.9}S$ QDs suggests the predominant nature of bridging (Δ = 134 and 112) over bidentate (Δ = 99) bonding mode of the carboxylate ligands. With a growing Cd content, unidentate coordination in QDs probably increases, e.g. for $Cd_{0.9}Zn_{0.1}S$ sample Δ = 124, 102 and 89. Comparing each ATR spectrum of $Cd_xZn_{1-x}S$ QDs, the only difference in the intensities of bands corresponding to vibrations modes of organic ligands was found. The difference in signal intensity is associated with the total content of the organic shell of the QDs, which in turn directly depends on their size.

By studying the ATR spectra of nanopowders of the composition $Cd_{0.2}Zn_{0.8}S$ (**Fig. 3b**), prepared with different ratios of Cd, Zn : S precursors, more significant differences were found. The positions of asymmetric and symmetric COO- stretching vibrations are very close to the positions of the corresponding vibrations in $Cd_xZn_{1-x}S$ samples; Δ values again suggest bridging and bidentate coordination of linoleate ligands. However, with an increase of the sulphur precursor ratio in the Cd, Zn : S series, a sequential decrease in the intensity of the band corresponding to metal carboxylates and new absorbance bands at 3124, 3204 cm^{-1} and shoulder at 3320 cm^{-1} can be observed. These new bands are characteristic for N-H stretching vibration modes. This phenomenon indicates a gradual change in the ligand in the protective shell of QDs.

During the interaction of the starting components, i.e. metal linoleates and an equimolar amount or lack of N-phenylmorpholine-4-carbothioamide, a nanocrystal with a protective shell of the same metal linoleates is formed. When an excess of sulphur source is introduced into the reaction mixture, the protective shell is forced to react with trisubstituted thiourea and at the same time, the concentration of metal linoleates reaches a possible minimum. Oleylamine, capable of coordination with metals, gradually displaces the leaving carboxylates in the protective shell. Thus, with an increasing ratio of trisubstituted thiourea to metal carboxylates, the ligand forming the protective shell of QDs is consequentially replaced, which is visible in FT-IR spectra (**Fig. 3b**).

ATR spectra of Cd-Zn-S QDs in the region 50 - 370 cm^{-1} are demonstrated in **Figure 4 a, b**. In the case of Cd-Zn-S samples, a dominant absorbance band with maxima between 287 and 248 cm^{-1} can be observed in the spectra. The increase of the intensity for the higher Cd content in the region of lower wavenumbers was detected, but it may be influenced by the background due to the lower sensitivity of the detector in this area. It is evident that spectra were formed by overlapping of several bands. Therefore, ATR spectra in the region 150 - 370 cm^{-1} have been deconvoluted into several separate individual bands (**Fig. 4a**).

In the case of $Cd_{0.1}Zn_{0.9}S$ and $Cd_{0.25}Zn_{0.7}5S$ QDs, the band centred at ~ 287 cm^{-1} was decomposed into four bands: strong and medium bands at 287 and 230 cm^{-1} and two bands with small intensity at 261 and 337 cm^{-1}. These bands can be associated with transverse optical (TO), transversal acoustical (TA), longitudinal acoustical (LA) and longitudinal optical (LO) phonon modes in cubic ZnS [38-40]. With an increase of Cd content in $Cd_xZn_{1-x}S$ QDs, all bands are shifted towards lower wavenumbers and new bands appear.

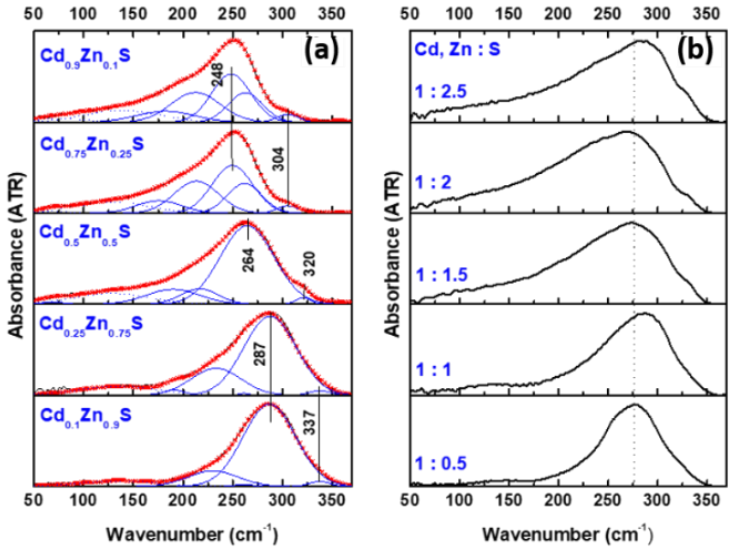

Figure 4. FT-IR deconvoluted ATR absorbance spectra of $Cd_xZn_{1-x}S$ QDs (a) and ATR absorbance spectra of $Cd_{0.2}Zn_{0.8}S$ QDs (b).

ATR spectra of $Cd_{0.9}Zn_{0.1}S$ and $Cd_{0.75}Zn_{0.25}S$ QDs were decomposed into five bands at 182, 212, 248, 262 and 304 cm^{-1}. These frequencies are in good agreement with characteristic phonon frequencies found in far-infrared absorbance and reflection spectra of bulk CdS with hexagonal structure [40,41]. In the case of $Cd_{0.5}Zn_{0.5}S$ QDs, the maxima of the main band at 264 cm^{-1} is located exactly in the middle between the transverse mode of cubic ZnS (287 cm^{-1}) and hexagonal CdS (248 cm^{-1}). A similar tendency applies to longitudinal modes. Therefore, we believe that relatively wide bands in decomposed spectra of $Cd_{0.5}Zn_{0.5}S$ QDs (e.g. at 264 and 320 cm^{-1}) do not correspond only to one mode but overlap smaller bands of transverse and longitudinal modes of both cubic and hexagonal structures. ATR spectra of $Cd_{0.2}Zn_{0.8}S$ QDs with different Cd, Zn : S ratio are displayed in **Figure 4b**. These spectra are close to the ATR spectra of $Cd_{0.1}Zn_{0.9}S$ and $Cd_{0.25}Zn_{0.75}S$ samples. A very small maximum shift near 280 cm^{-1} is probably due to different sizes of QDs. Depending on the position of this maximum, the cubic structure of nanoparticles may be presumed.

3.3.2 XRD analysis and morphology of Cd-Zn-S QDs

In order to investigate the crystal structure, powder X-Ray diffraction (XRD) analysis was performed on Cd-Zn-S QDs. The XRD patterns for $Cd_{0.2}Zn_{0.8}S$ QDs (**Fig. 5a**) with different Cd, Zn: S ratio exhibit three broad prominent Bragg reflections which can be indexed as (111), (220) and (311) planes. These reflections confirm the dominant cubic zinc blende (ZB) structure of the bulk ZnS phase (ICSD:671466) with a space group $F\bar{4}3m$. The broadening of diffraction peaks reflects

the nanocrystalline nature of $Cd_{0.2}Zn_{0.8}S$ QDs. As can be seen, the characteristic peaks of $Cd_{0.2}Zn_{0.8}S$ QDs are located between main diffraction peaks of ZnS (ICSD:671466) and CdS bulk materials (ICSD:186009) what confirms the formation of alloyed $Cd_{0.2}Zn_{0.8}S$ QDs. It is evident from the XRD spectra that there are no other peaks from impurities or secondary phases. With an increase of the sulphur precursor amount in the starting reaction mixture, a gradual peak shift toward higher angles was observed. In our opinion, during the interaction of equimolar amounts of the starting components, the distribution of elements in the QD is close to homogeneous. Nevertheless, the reactivity of cadmium salt is slightly higher than that one of zinc. Therefore, the protective shell of QDs mainly consists of zinc linoleate. When an excessive amount of trisubstituted thiourea is introduced, an enriched ZnS outer layer is created at the intermediate stages of growth. This layer is formed from an organometallic shell, as well as from free metal carboxylates in the reaction mixture. Thus, additionally formed QDs' layers predominantly consist of zinc sulphide, which is reflected in the peaks' shift in the XRD patterns (**Fig. 5a**). Also, it could be noticed an appearance of the small contribution of the wurtzite (WZ) phase in the structure of $Cd_{0.2}Zn_{0.8}S$ QDs starting from the Cd, Zn : S ratio = 1 : 1.5. This phenomenon called polytypism was described in the literature [42]. Such a transformation of ZB to WZ structure could happen due to the low internal energy differences (< 20 meV per atom) between the two phases. Because of the peak's width, (111) crystal planes of $Cd_{0.2}Zn_{0.8}S$ QDs (ZB phase) could overlap with the (100), (002) and (101) planes of the WZ phase. The estimated crystallite sizes were calculated according to the Scherrer's equation [32]. The calculated lattice parameters and the average crystal sizes of $Cd_{0.2}Zn_{0.8}S$ QDs are presented in **Table 1**.

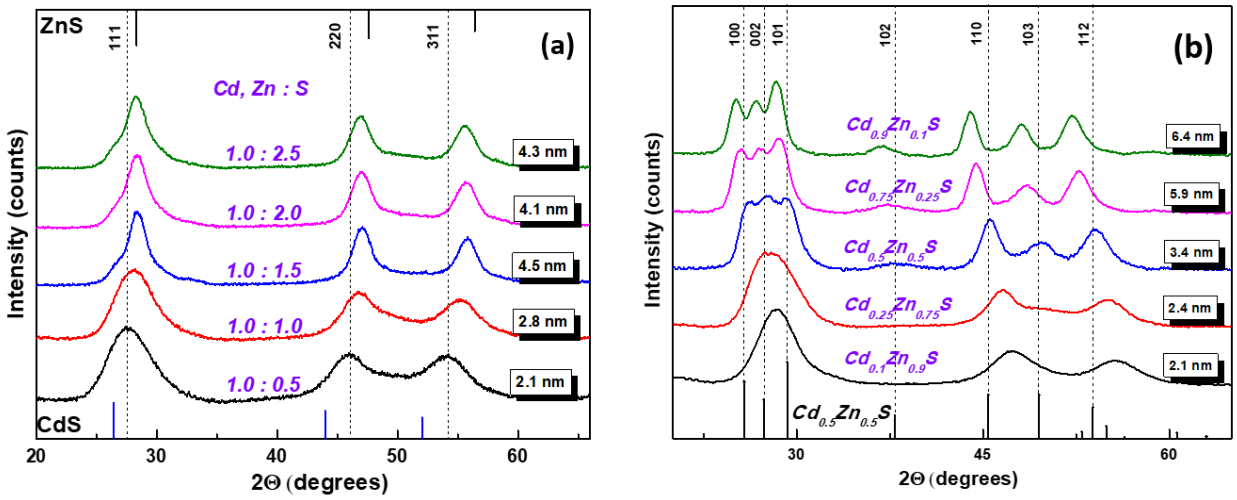

Figure 5. Powder XRD patterns of Cd-Zn-S QDs. Peaks' positions from the bulk ZnS, CdS (a) and $Cd_{0.5}Zn_{0.5}S$ (b) are given as a reference from the database.

XRD analysis of $Cd_xZn_{1-x}S$ QDs with different Cd : Zn ratio revealed 2 types of the crystal structure (Fig. 5b). According to XRD patterns, with an increase of Cd content in the $Cd_xZn_{1-x}S$ QDs, a gradual shift of main diffraction peaks to lower angles and crystallographic phase change from ZB structure to WZ structure was observed. Powder XRD patterns of $Cd_{0.1}Zn_{0.9}S$ and $Cd_{0.25}Zn_{0.75}S$ QDs exhibit 3 main peaks at 2θ values of 27.6, 46.1 and 54.1, which can be assigned with (111), (220), and (311) crystallographic planes of cubic structure with a space group $F\bar{4}3m$.

Table 1. Structural parameters of $Cd_{0.2}Zn_{0.8}S$ QDs (different Cd, Zn : S precursor ratios)

QDs parameters	Cd, Zn : S precursor ratios				
	1 : 0.5	**1 : 1**	**1 : 1.5**	**1 : 2**	**1 : 2.5**
Space group	$F\bar{4}3m$	$F\bar{4}3m$	$F\bar{4}3m$	$F\bar{4}3m$	$F\bar{4}3m$
Average crystalline size, nm	2.1	2.8	4.5	4.1	4.3
Cubic lattice parameters *a*=*b*=*c*, Å	5.57	5.52	5.47	5.47	5.49

In the XRD spectra of $Cd_{0.5}Zn_{0.5}S$, $Cd_{0.75}Zn_{0.25}S$ and $Cd_{0.9}Zn_{0.1}S$ QDs, 7 characteristic peaks at 2θ values of 25.1, 26.6, 28.2, 36.8, 43.9, 48.1 and 56.1, were determined and indexed to the (100), (002), (101), (102), (110), (103) and (112) crystallographic planes of hexagonal structure with a space group $P6_3cm$. Sequential incorporation of Cd into the ZnS lattice leads to the partial replacement of smaller Zn^{2+} ion (0.74 Å) by the bigger Cd^{2+} ion (0.97 Å) and consequently to the expansion of the unit cell and increase the size of QDs (see **Table 2**). Such behaviour is in good agreement with the literature [43].

Table 2. Structural parameters of $Cd_xZn_{1-x}S$ QDs (different Cd : Zn precursor ratios)

QDs parameters	Cd : Zn precursor ratios				
	0.1 : 0.9	**0.25 : 0.75**	**0.5 : 0.5**	**0.75 : 0.25**	**0.9 : 0.1**
Cubic phase ($F\bar{4}3m$), %	100	84.8	67.7	24.1	0
Hexagonal phase ($P6_3cm$), %	0	15.2	32.3	75.9	100
Average crystalline size, nm	2.1	2.4	3.4	5.9	6.4
Cubic lattice parameters *a*=*b*=*c*, Å	5.46	5.55	5.64	5.76	-
Hexagonal lattice parameters *a*=*b*, Å	-	3.88	3.99	4.09	4.13
Hexagonal lattice parameters *c*, Å	-	6.45	6.53	6.66	6.72

STEM images of the synthesized $Cd_{0.2}Zn_{0.8}S$ QDs and $Cd_xZn_{1-x}S$ QDs are depicted in **Figure 6** and **Figure 7**, respectively. The typical $Cd_{0.2}Zn_{0.8}S$ QDs prepared with deficiency or excess of the sulphur precursor possess a uniform sphere-like morphology. It should be noticed that with an increase of the sulphur precursor amount (in case of $Cd_{0.2}Zn_{0.8}S$ QDs) (**Fig. 6**) or Cd content (in case of $Cd_xZn_{1-x}S$ QDs) (**Fig. 7**), the average size of nanocrystals observably grows but uniformity and sphere-like shape remain constant. These values are comparable with the calculated one from XRD data. The elemental composition of all as-synthesized Cd-Zn-S QDs series was characterized using EDS analysis. The EDS spectra of all Cd-Zn-S QDs confirm the presence of Zn, Cd, S elements in desired composition of QDs. Also, the appearance of carbon and oxygen signals in the EDS data were detected because of the organic ligands forming the protective shell of the samples. All data from the elemental analysis are listed in **Table 3**.

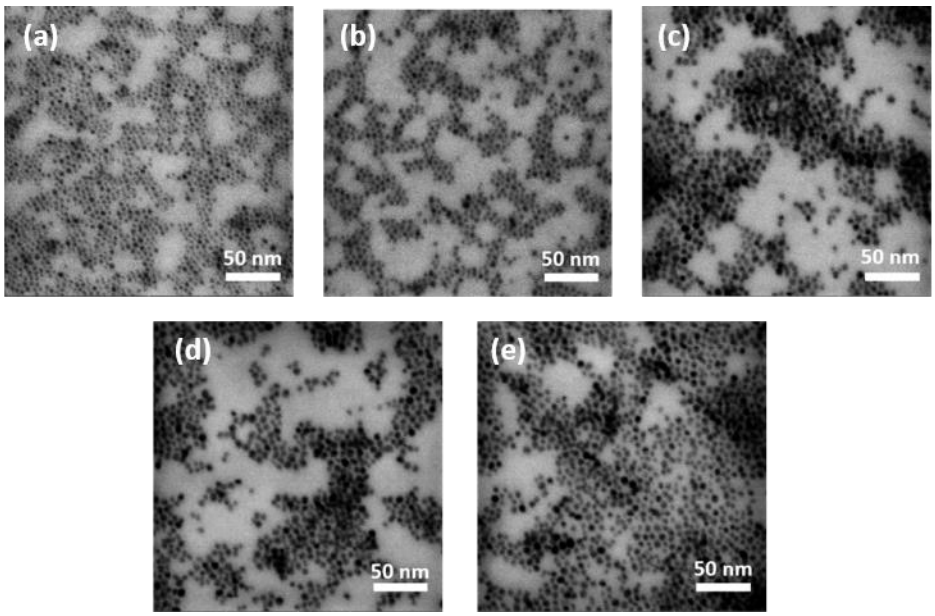

Figure 6. STEM images of $Cd_{0.2}Zn_{0.8}S$ QDs, prepared with different Cd, Zn : S precursors ratios a) 1 : 0.5; b) 1 : 1; c) 1 : 1.5; d) 1 : 2; e) 1 : 2.5.

Table 3. Elemental composition of Cd-Zn-S QDs measured by EDS

Composition	Cd, at.%	Zn, at.%	S, at.%	Cd : Zn ratio	Cd, Zn : S ratio
Cd, Zn : S precursors ratio **1 : 0.5**	11.1	46.0	42.9	19.4 : 80.6	57.1 : 42.9
1 : 1	11.7	44.9	43.4	20.7 : 79.3	56.6 : 43.4
1 : 1.5	9.6	43.1	47.3	18.2 : 81.8	52.7 : 47.3
1 : 2	9.9	41.2	48.9	19.4 : 80.6	51.1 : 48.9
1 : 2.5	10.2	40.2	49.6	20.2 : 79.8	50.4 : 49.6
Cd : Zn precursors ratio **0.1 : 0.9**	5.7	55.5	38.8	9.3 : 90.7	61.2 : 38.8
0.25 : 0.75	14.2	41.4	44.4	25.5 : 74.5	55.6 : 44.4
0.5 : 0.5	25.7	28.6	45.7	47.3 : 52.7	54.3 :45.7
0.75 : 0.25	40.5	14.4	45.1	73.8 : 26.2	54.9 : 45.1
0.9 : 0.1	50.6	4.2	45.2	92.2 : 7.8	54.8 : 45.2

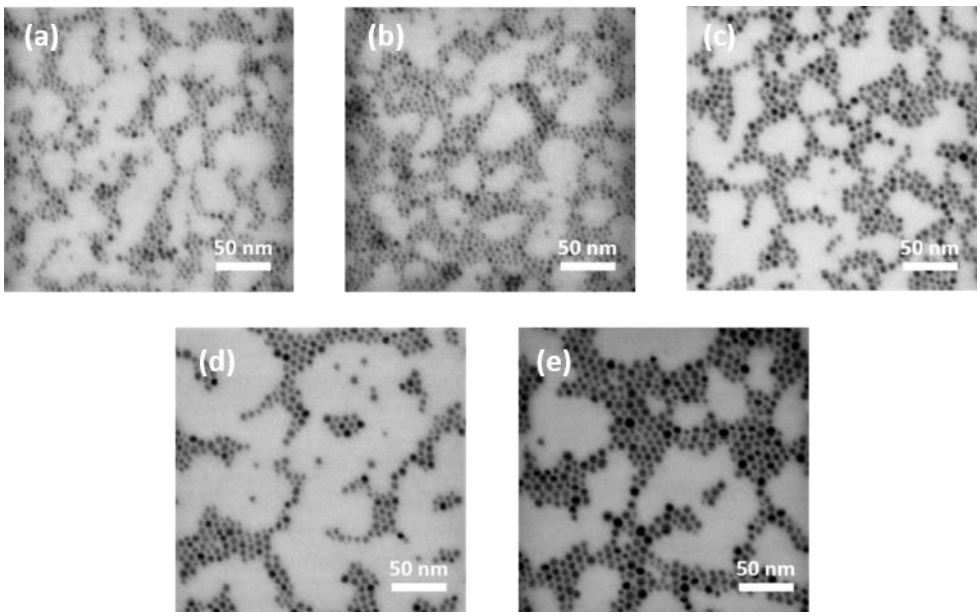

Figure 7. STEM images of $Cd_xZn_{1-x}S$ QDs prepared with different Cd : Zn precursors ratios a) $Cd_{0.1}Zn_{0.9}S$ QDs; b) $Cd_{0.25}Zn_{0.75}S$ QDs; c) $Cd_{0.5}Zn_{0.5}S$ QDs; d) $Cd_{0.75}Zn_{0.25}S$ QDs; e) $Cd_{0.9}Zn_{0.1}S$ QDs.

3.3.3 X-Ray Photoelectron Spectroscopy

X-Ray Photoelectron Spectroscopy (XPS) was performed to study the atoms surrounding and the elemental composition on the surface of two series of synthesized ternary Cd-Zn-S QDs. Calibration of the binding energy values was carried out relative to the position of the C 1s peak (284.8 eV) taken as a reference [44-47]. The XPS survey spectra (1500 - 0 eV) for Cd-Zn-S QDs with different Cd, Zn : S ratios are presented in **Figure 8a**. It is noteworthy that the intensity of the signals corresponding to metals and sulphur for this series of QDs is not affected by a change of Cd, Zn and S amount. However, there is a significant difference in the ratios of the elements which formed the QD's protective shell. A gradual decrease in the relative signal intensity of O 1*s* occurs due to a decrease in the number of carboxylates moieties in the organic shell of QDs. A similar dependence in the gradual replacement of carboxylates with OAm in the protective shell of QD was found in the FT-IR spectra.

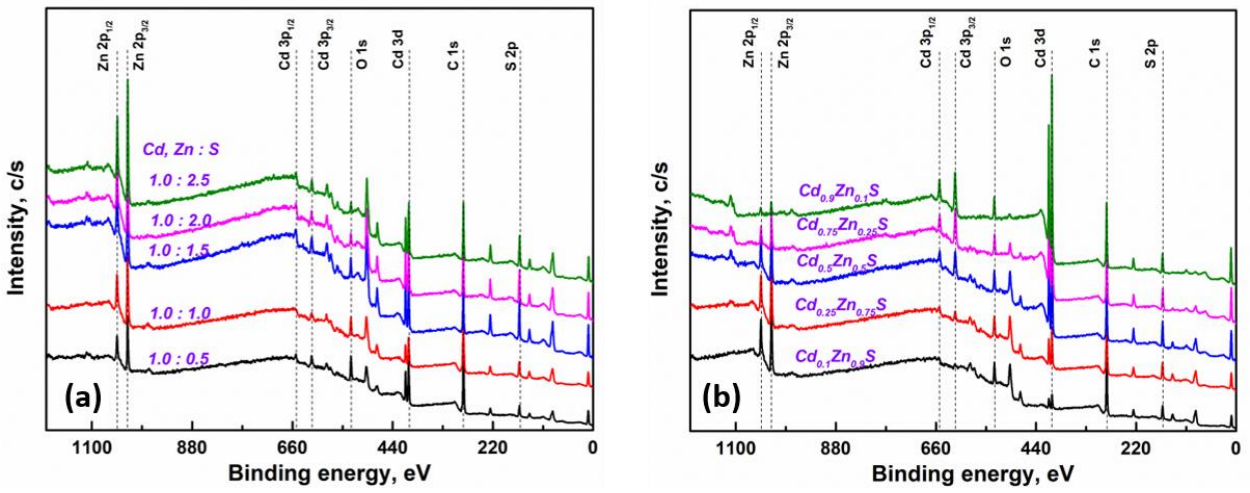

Figure 8. XPS survey spectra of ternary Cd-Zn-S QDs.

As it follows from the survey spectra for the $Cd_xZn_{1-x}S$ QDs series with different Cd : Zn ratios (**Fig. 8b**), a change in the peak intensities corresponding to metals with a constant position of the signals of all elements was observed. With an increase in the amount of Cd in $Cd_xZn_{1-x}S$ QDs, the intensities of the Cd $3p_{1/2}$, Cd $3p_{3/2}$ and Cd $3d$ doublet peaks increase significantly, whereas the intensities of the Zn $2p_{1/2}$ and Zn $2p_{3/2}$ peaks decrease. The intensity of the S $2p$ peak remains unchanged. Such a change in the signal intensities of the elements correlates with the ratios taken to the reaction and may indicate the homogeneity and conformity of the elemental composition of the synthesized QDs. Also, the intensity of the O $1s$ and C $1s$ peaks remains the same, which indicates that the organic shell is similar for all $Cd_xZn_{1-x}S$ QDs and does not depend on the Cd : Zn ratio.

3.4 Optical properties of CdZnS QDs

The electronic transition frequencies can be controlled by changing several factors such as the elemental composition of a semiconductor QDs, its shape and size. In the case of multicomponent compositions, the influence of the nucleation conditions and growth of QDs is much wider and affects not only the size and shape of QDs, but also the elements' distribution in the nanocrystal. Depending on the nature of the reacting compounds, spontaneous nucleation may occur at rather low temperatures. Further growth shall be determined by the reactivity of the starting components. The multistep interaction of trisubstituted thiourea with metal carboxylates determines the formation of the complex compound and the decomposition of this complex to mixed sulphide. In our opinion, this process occurs at the same rate for both linoleates. But still, the question about the difference in decomposition-formation rates of cadmium and zinc sulphides remains open. To the best of our knowledge, the interaction of non-equimolar amounts of reagents in this process has not been previously studied.

The photoluminescence spectra of $Cd_{0.2}Zn_{0.8}S$ QDs series were measured to obtain information about the optical properties and their correlation with structural features (**Fig. 9a**). The assignment of these PL spectra with the position of the first exciton in the absorbance spectra is presented in the form of the Stokes shift (**Fig. 9b**). As follows from the normalized PL spectra of $Cd_{0.2}Zn_{0.8}S$ QDs, the position of the PL maximum (PL_{max}) does not match for $Cd_{0.2}Zn_{0.8}S$ QDs obtained with different ratios of precursors. With the equimolar ratio Cd, Zn : S, the PL_{max} is observed at 405 nm, which corresponds to the data presented earlier [32]. For $Cd_{0.2}Zn_{0.8}S$ QDs obtained with a deficiency (Cd, Zn : S = 0.5) or a slight excess (Cd, Zn : S = 1.5) of trisubstituted thiourea, a slight red shift of the PL_{max} of the spectrum is observed (from 405 nm to 412 nm and 424 nm, respectively) (**Fig. 9a, b**). The position of PL_{max} for the $Cd_{0.2}Zn_{0.8}S$ QDs synthesized with the large excess of trisubstituted thiourea remains the same as for the equimolar ratios of the starting components. This phenomenon can be explained by the difference in the formation rates of Cd and Zn sulphides, which in turn is significantly affected by an excess of one of the components in the process. The $Cd_{0.2}Zn_{0.8}S$ QDs synthesized in a deficiency of a sulphur precursor are characterized by a wide emission band in 480 - 600 nm range in addition to the main PL signal at 405 nm. This phenomenon is related to the recombination of charge carriers localized on surface defects of $Cd_{0.2}Zn_{0.8}S$ QDs. For the other $Cd_{0.2}Zn_{0.8}S$ QDs synthesized with the larger amounts of trisubstituted thiourea, this long-wavelength band disappeared. A subsequent increase in the amount of sulphur source in the synthesis of QDs leads to the passivation of their

surface. The positions of the first exciton in the ABS spectra are changing similar to the position of the PL_{max} of $Cd_{0.2}Zn_{0.8}S$ QDs obtained with different ratios of the precursors. Therefore, the Stokes shift values (**Fig. 9b**, **Table 4**) are in the range of 27 nm ± 6 nm.

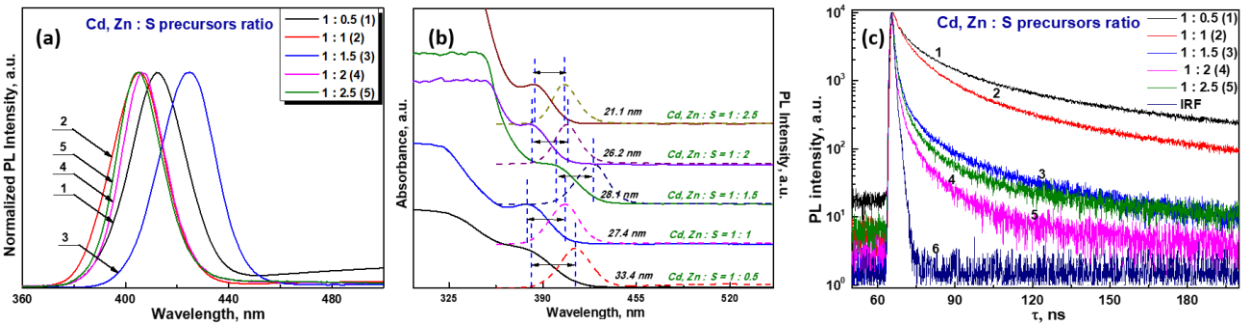

Figure 9. Optical properties: PL spectra of $Cd_{0.2}Zn_{0.8}S$ QDs (a); comparison of ABS (solid lines) and emission spectra (dashed lines) of ternary $Cd_{0.2}Zn_{0.8}S$ QDs (b); PL decay kinetics curves $Cd_{0.2}Zn_{0.8}S$ QDs (c).

Table 4. Optical properties of synthesized $Cd_{0.2}Zn_{0.8}S$ QDs. Peak maximum of the emission in photoluminescence spectra (λ_{PL}), peak maximum of the first exciton in the absorbance spectra (λ_{ABS}), full width at half maximum of the photoluminescence band (FWHM), Stokes shift, band gap (E_g), relative PL QY

Cd, Zn : S ratios	PL and ABS characteristics					
	λ_{PL}, nm	λ_{ABS}, nm	FWHM, nm	Stokes shift, nm	Band gap E_g, eV	PL QY, %
1 : 0.5	412	379	31	33.4	3.06	65
1 : 1	405	378	24	27.4	3.09	70
1 : 1.5	424	396	27	28.1	2.95	54
1 : 2	407	381	27	26.2	3.10	48
1 : 2.5	405	384	27	21.1	3.09	47

Considering Cd-Zn-S QDs as direct band gap semiconductors we can approximate the spectral dependence of the absorbance coefficient close to band gap energy by Tauc relation [48] in the form:

$$(\alpha hv) \sim (hv - E_g)^{1/2}\,, \qquad (1)$$

where hv is incident photon energy. The E_g value is then obtained by linear extrapolation of nearly linear $(\alpha hv)^2$ dependence in the UV part of the spectra. The intersection of this extrapolated line with hv axis gives the value of E_g and these values are presented in **Tables 4, 6**. The relative PL QY was calculated according to the formula:

$$PL\ QY_{QD} = PL\ QY_{ref} \frac{PL_{QD}}{PL_{ref}} \frac{ABS_{ref}}{ABS_{QD}} \frac{n_{CHCl_3}}{n_{ethanol}}\,, \qquad (2)$$

where ABS_{QD} and ABS_{ref} are optical densities at the certain excitation wavelength and the refractive indices (n) of the solvents, $PL\ QY_{QD}$ is the PL quantum yield of synthesized QDs, $PL\ QY_{ref}$ is the PL quantum yield of Coumarin 334 as a reference ($PL\ QY_{ref}$ = 0.69 in ethanol) [49].

In the PL decay kinetics of $Cd_{0.2}Zn_{0.8}S$ QDs, a certain dependence on the Cd, Zn : S ratios taken to the synthesis is also observed. The PL decay kinetics curves $Cd_{0.}2Zn_{0.8}S$ QDs were measured under pulsed excitation at 362 nm and recording at the PL_{max} (**Fig. 9c**). The PL decay kinetics curves were fitted using the three-exponential function *I(t)* re-convoluted with the instrument response function (*IRF*) (**Eq. 3**). The *IRF* was measured using LUDOX aqueous solution.

$$I(t) = \int_0^t IRF(t') \left(C + \sum_{i=1}^{3} A_i \exp\left(-\frac{t-t'}{\tau_i} \right) \right) dt' \quad , \tag{3}$$

where τ_i and A_i are photoluminescence decay time (PL lifetime) and amplitudes [45].
The average PL lifetime was calculated using **Eq. 4** [45]. Data processing results are presented in **Table 5**.

$$\tau_{avg} = \frac{\sum_{i=1}^{3} A_i \tau_i}{\sum_{i=1}^{3} A_i}, \tag{4}$$

The presence of three components in the PL decay kinetics of ternary QDs has been observed by many authors [22,44,50,51]. The presence of several temporal components of the PL decay curves is associated with the existence of different carrier recombination paths in these QDs [50]. The "fast" decay time component (τ_1) refers to the process of recombination charge carriers from shallow traps, while the longer decay time (τ_2) is associated with the charge carrier's recombination from the deeper defects' levels (deep traps) [52]. The presence of the third and the longest time component (τ_3) is related to the recombination of surface localized charge carriers. According to **Table 5**, a shift in the Cd, Zn : S ratio towards the excess of sulphur leads to a decrease in the average PL lifetime (τ_{avg}) of $Cd_{0.2}Zn_{0.8}S$ QDs. The longest average PL lifetime is observed for $Cd_{0.2}Zn_{0.8}S$ QDs synthesized with a deficiency of a sulphur source. The same trend was demonstrated by other authors as well [53].

Table 5. Summary of $Cd_{0.2}Zn_{0.8}S$ QDs PL lifetime measurements. Time constants τ_1, τ_2 and τ_3; amplitude components A_1, A_2 and A_3 and PL average lifetime τ_{avg}

Cd, Zn : S ratios	λ_{em}, nm	τ_1, ns	τ_2, ns	τ_3, ns	A_1	A_2	A_3	τ_{avg}, ns
1 : 0.5	412	0.97	12.01	89.81	0.6809	0.2344	0.0847	11.08
1 : 1	405	1.12	9.41	63.41	0.7008	0.2572	0.0419	5.86
1 : 1.5	424	0.35	5.03	45.57	0.9593	0.0368	0.0039	0.70
1 : 2	407	0.04	2.93	17.19	0.9958	0.0037	0.0006	0.06
1 : 2.5	405	0.15	3.54	28.35	0.9848	0.0135	0.0017	0.25

As mentioned above, an increase in the amount of sulphur source in the synthesis of QDs can lead to passivation of the surface and a decrease in the number of surface defects. This, in turn, increases the efficiency of the trapping process for shallow and deep traps and increases the probability of nonradiative carrier recombination paths, which leads to a decrease in the average PL decay time of $Cd_{0.2}Zn_{0.8}S$ QDs.

Figure 10 illustrates the emission, absorbance, and decay kinetics PL spectra for $Cd_xZn_{1-x}S$ QDs. It should be noted that with an increase of the Cd content in the nanomaterials, the PL_{max}

shifts to the red region of the spectrum (**Fig. 10a**), overlapping almost the entire visible region. Such shift is caused by a decrease in the band gap of $Cd_xZn_{1-x}S$ QDs. Also, the obtained $Cd_xZn_{1-x}S$ QDs have rather narrow emission bands (FWHM is in the order of 20 nm) at significant Stokes shift values (≈ 25 nm), see **Table 6**. These parameters of $Cd_xZn_{1-x}S$ QDs allow them to be promising candidates for use in medicine as biomarkers [54,55] and the production of LEDs [56,57].

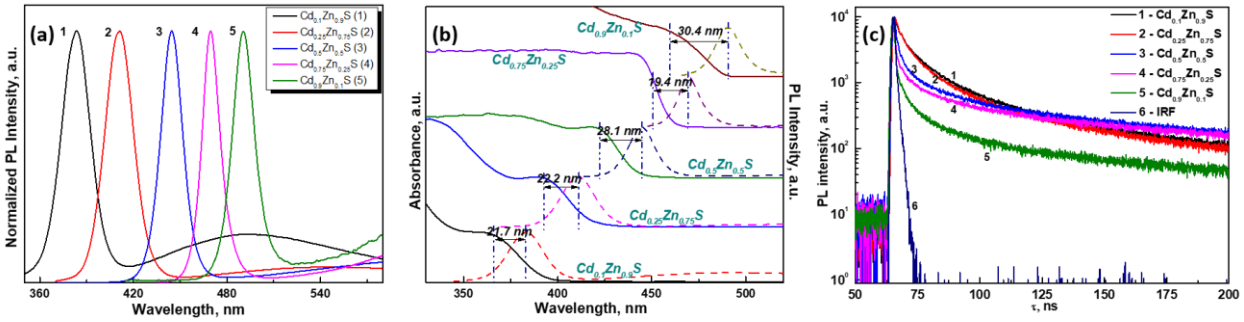

Figure 10. Optical properties: PL spectra of $Cd_xZn_{1-x}S$ QDs (a); comparison of ABS (solid lines) and emission spectra (dashed lines) of ternary $Cd_xZn_{1-x}S$ QDs (b); PL decay kinetics curves $Cd_xZn_{1-x}S$ QDs (c).

Table 6. Optical properties of synthesized $Cd_xZn_{1-x}S$ QDs. Peak maximum of the emission in photoluminescence spectra (λ_{PL}), peak maximum of the first exciton in the absorbance spectra (λ_{ABS}), full width at half maximum of the photoluminescence band (FWHM), Stokes shift, band gap (E_g), relative PL QY

Cd : Zn ratios	PL and ABS characteristics					
	λ_{PL}, nm	λ_{ABS}, nm	FWHM, nm	Stokes shift, nm	Band gap E_g, eV	PL QY, %
0.1 : 0.9	384	362	23	21.7	3.21	68
0.25 : 0.75	411	389	25	22.2	3.01	70
0.5 : 0.5	445	417	19	28.1	2.84	65
0.75 : 0.25	469	450	15	19.4	2.72	46
0.9 : 0.1	491	461	18	30.4	2.57	38

An important characteristic of QDs as scintillators is their PL lifetime. The PL decay kinetics of $Cd_xZn_{1-x}S$ QDs were measured upon pulsed excitation by laser diodes (LEDs) at 362 nm and 391 nm and registration at the PL_{max} (**Fig. 10c**). For the all QDs presented in this paper, the PL decay kinetics curves are multi-exponential and consist of three components. The first two components relate to the recombination of charge carriers from shallow and deep traps, and the third component is associated with the recombination of surface localized charge carriers. The fitting of the $Cd_xZn_{1-x}S$ QDs PL decay kinetics curves was carried out according to **Eq. 3**, and the average PL lifetime (τ_{avg}) was calculated using **Eq. 4** (see **Table 7**).

Table 7. Summary of $Cd_xZn_{1-x}S$ QDs PL lifetime measurements. Time constants τ_1, τ_2 and τ_3; amplitude components A_1, A_2 and A_3 and PL average lifetime τ_{avg}

Cd : Zn ratios	λ_{em}, nm	τ_1, ns	τ_2, ns	τ_3, ns	A_1	A_2	A_3	τ_{avg}, ns
0.1 : 0.9	362	1.04	9.74	61.78	0.7017	0.2558	0.0426	5.85
0.25 : 0.75	362	1.12	9.60	63.29	0.7223	0.2406	0.0371	5.46
0.5 : 0.5	362	0.39	7.99	94.85	0.9287	0.0544	0.0169	2.40
0.75 : 0.25	391	0.22	8.54	114.69	0.9667	0.0246	0.0086	1.42
0.9 : 0.1	391	0.01	6.03	78.51	0.9955	0.0039	0.0006	0.08

An increase of Cd content in $Cd_xZn_{1-x}S$ QDs leads to changes in the PL decay kinetics curves (**Fig. 10c**). It should be noted from PL decay kinetic curves, the "fast" time components (τ_1, τ_2) decrease and the "slow" time component (τ_3) slightly increases, which is supported by fitting data (**Table 7**). At the same time, the intensity of the "fast" components increases, while the intensity of the "slow" component decreases, which leads to a general decrease in the average PL lifetime. The reduction of the two "fast" time components in the PL decay kinetics of $Cd_xZn_{1-x}S$ QDs can be associated with the appearance of a larger number of defects inside the QDs with an increase of Cd content in the sample. Due to the difference in the atomic radii of Zn and Cd (0.74 Å and 0.92 Å respectively), their mutual substitution in the QD can lead to the formation of internal defects. Consequently, the probability of a nonradiative relaxation path through internal defects increases following the reduction in the "fast" time components in the PL decay kinetics of $Cd_xZn_{1-x}S$ QDs.

4. Conclusions

The ternary alloyed Cd-Zn-S QDs with compositional distribution close to homogeneous limit were obtained using N-phenylmorpholine-4-carbothioamide as a novel sulphur source in a non-coordinating solvent. Based on our previous research, we investigated the effect of deficiency and excess of the trisubstituted thiourea on the structure and optical properties of synthesized $Cd_{0.2}Zn_{0.8}S$ QDs. Based on analytical data, it was found that with the significant excess of the sulphur precursor, *co*-ligand oleylamine partially or completely compensates metal linoleates in the protective shell of QDs. This work has revealed a strong influence of the synthesis conditions and the ratios of the starting components on the size and chemical composition of the QDs, on the formation of the protective shell and, as a consequence, on the optical properties of the nanomaterials. $Cd_xZn_{1-x}S$ QDs synthesized with various metal linoleates ratios exhibit tunable emission covering almost the entire visible spectrum range. The findings of the study demonstrate that homogeneous in shape and size, highly photoluminescent (PL QY up to 70 %) and high colour purity (FWHM < 31 nm) Cd-Zn-S QDs with an average size of 2.1 to 6.4 nm can be easily prepared with the involvement of available and environmentally friendly trisubstituted thiourea. We have obtained comprehensive results demonstrating the possibility to transfer this approach to the large-scale production, due to the high reproducibility, reliability and safety of the presented method.

Declaration of competing interest

The authors declare that they have no known competing financial interests or personal relationships that could have appeared to influence the work reported in this paper.

Acknowledgments

Authors appreciate financial support from project “High-sensitive and low-density materials based on polymeric nanocomposites” - NANOMAT (№ CZ.02.1.01/0.0/0.0/17_048/0007376), support from the grants LM2018103 and ED4.100/11.0251 from the Ministry of Education, Youth and Sports of the Czech Republic and European Regional Development Fund-Project “Modernization and upgrade of the CEMNAT” (№ CZ.02.1.01/0.0/0.0/16_013/0001829).

References

[1] Q. Sun, Y.A. Wang, L.S. Li, D. Wang, T. Zhu, J. Xu, C. Yang, Y. Li, Bright, multicoloured light-emitting diodes based on quantum dots, Nat. Photonics. 1 (2007) 717–722. doi:10.1038/nphoton.2007.226.

[2] S. Slang, L. Loghina, K. Palka, M. Vlcek, Exposure enhanced photoluminescence of $CdS_{0.9}Se_{0.1}$ quantum dots embedded in spin-coated $Ge_{25}S_{75}$ thin films, RSC Adv. 7 (2017) 53830–53838. doi:10.1039/c7ra09540f.

[3] X. Jin, H. Li, S. Huang, X. Gu, H. Shen, D. Li, X. Zhang, Q. Zhang, F. Li, Q. Li, Bright alloy type-II quantum dots and their application to light-emitting diodes, J. Colloid Interface Sci. 510 (2018) 376–383. doi:10.1016/j.jcis.2017.09.080.

[4] I.L. Medintz, H.T. Uyeda, E.R. Goldman, H. Mattoussi, Quantum dot bioconjugates for imaging, labelling and sensing, Nat. Mater. 4 (2005) 435–446. doi:10.1038/nmat1390.

[5] L. Pagano, F. Pasquali, S. Majumdar, R. De La Torre-Roche, N. Zuverza-Mena, M. Villani, A. Zappettini, R.E. Marra, S.M. Isch, M. Marmiroli, E. Maestri, O.P. Dhankher, J.C. White, N. Marmiroli, Exposure of: Cucurbita pepo to binary combinations of engineered nanomaterials: Physiological and molecular response, Environ. Sci. Nano. 4 (2017) 1579–1590. doi:10.1039/c7en00219j.

[6] S. Das, B.P. Wolfson, L. Tetard, J. Tharkur, J. Bazata, S. Santra, Effect of N-acetyl cysteine coated CdS:Mn/ZnS quantum dots on seed germination and seedling growth of snow pea (Pisum sativum L.): Imaging and spectroscopic studies, Environ. Sci. Nano. 2 (2015) 203–212. doi:10.1039/c4en00198b.

[7] E. Guo, L. Yin, L. Zhang, CdS quantum dot sensitized anatase TiO_2 hierarchical nanostructures for photovoltaic application, CrystEngComm. 16 (2014) 3403–3413. doi:10.1039/c4ce00019f.

[8] C. Liu, Z. Li, T.J. Hajagos, D. Kishpaugh, D.Y. Chen, Q. Pei, Transparent Ultra-High-Loading Quantum Dot/Polymer Nanocomposite Monolith for Gamma Scintillation, ACS Nano. 11 (2017) 6422–6430. doi:10.1021/acsnano.7b02923.

[9] W. Yang, T. Bin, H. Heyong, L. Bin, T. Ke, S. Yong, Y. Wei, C. Chao, The study of zinc sulphide scintillator for fast neutron radiography, Phys. Procedia. 43 (2013) 205–215.

doi:10.1016/j.phpro.2013.03.024.

[10] I.H. Campbell, B.K. Crone, Quantum-Dot/Organic Semiconductor Composites for Radiation Detection, Adv. Mater. 18 (2006) 77–79. doi:10.1002/adma.200501434.

[11] C. Dujardin, E. Auffray, E. Bourret-Courchesne, P. Dorenbos, P. Lecoq, M. Nikl, A.N. Vasil'ev, A. Yoshikawa, R.-Y. Zhu, Needs, Trends, and Advances in Inorganic Scintillators, IEEE Trans. Nucl. Sci. 65 (2018) 1977–1997. doi:10.1109/TNS.2018.2840160.

[12] E. Zanazzi, M. Favaro, A. Ficorella, L. Pancheri, G.F.D. Betta, A. Quaranta, Photoluminescence enhancement of colloidal CdSe/ZnS quantum dots embedded in polyvinyl alcohol after 2 MeV proton irradiation: crucial role of the embedding medium, Opt. Mater. (Amst). 88 (2019) 271–276. doi:10.1016/j.optmat.2018.11.047.

[13] A. Kongkanand, K. Tvrdy, K. Takechi, M. Kuno, P. V. Kamat, Quantum Dot Solar Cells. Tuning Photoresponse through Size and Shape Control of CdSe−TiO_2 Architecture, J. Am. Chem. Soc. 130 (2008) 4007–4015. doi:10.1021/ja0782706.

[14] I. Lokteva, N. Radychev, F. Witt, H. Borchert, J. Parisi, J. Kolny-Olesiak, Surface Treatment of CdSe Nanoparticles for Application in Hybrid Solar Cells: The Effect of Multiple Ligand Exchange with Pyridine, J. Phys. Chem. C. 114 (2010) 12784–12791. doi:10.1021/jp103300v.

[15] P. Eskandari, F. Kazemi, Z. Zand, Photocatalytic reduction of aromatic nitro compounds using CdS nanostructure under blue LED irradiation, J. Photochem. Photobiol. A Chem. 274 (2014) 7–12. doi:10.1016/j.jphotochem.2013.09.011.

[16] C.M. Bernt, P.T. Burks, A.W. Demartino, A.E. Pierri, E.S. Levy, D.F. Zigler, P.C. Ford, Photocatalytic carbon disulfide production via charge transfer quenching of quantum dots, J. Am. Chem. Soc. 136 (2014) 2192–2195. doi:10.1021/ja4083599.

[17] H. Zhang, Y. Zhang, Q. He, L. Liu, G. Ding, Z. Jiao, Mixed-solvothermal slow release synthesis of $Zn_xCd_{1-x}S_y$ nanorods with high visible light photocatalytic activities, CrystEngComm. 13 (2011) 6650. doi:10.1039/c1ce05548h.

[18] O. Wang, L. Wang, Z. Li, Q. Xu, Q. Lin, H. Wang, Z. Du, H. Shen, L.S. Li, High-efficiency, deep blue ZnCdS/$Cd_xZn_{1-x}S$/ZnS quantum-dot-light-emitting devices with an EQE exceeding 18%, Nanoscale. 10 (2018) 5650–5657. doi:10.1039/C7NR09175C.

[19] M. Yang, Y. Wang, Y. Ren, E. Liu, J. Fan, X. Hu, Zn/Cd ratio-dependent synthetic conditions in ternary ZnCdS quantum dots, J. Alloys Compd. 752 (2018) 260–266. doi:10.1016/j.jallcom.2018.04.084.

[20] A. Nath Bhatt, U.K. Verma, B. Kumar, Temporal evolution of white light emitting CdS core and $Cd_{1-x}Zn_xS$ graded shell quantum dots fabricated using single step non-injection technique, Opt. Mater. (Amst). 92 (2019) 143–149. doi:10.1016/j.optmat.2019.04.008.

[21] R. García-Rodríguez, M.P. Hendricks, B.M. Cossairt, H. Liu, J.S. Owen, Conversion reactions of cadmium chalcogenide nanocrystal precursors, Chem. Mater. 25 (2013) 1233–1249. doi:10.1021/cm3035642.

[22] M. Masab, H. Muhammad, F. Shah, M. Yasir, M. Hanif, Facile synthesis of CdZnS QDs:

Effects of different capping agents on the photoluminescence properties, Mater. Sci. Semicond. Process. 81 (2018) 113–117. doi:10.1016/j.mssp.2018.03.023.

[23] W.W. Yu, X. Peng, Formation of High-Quality CdS and Other II-VI Semiconductor Nanocrystals in Noncoordinating Solvents: Tunable Reactivity of Monomers, Angew. Chemie Int. Ed. 41 (2002) 2368–2371. doi:10.1002/1521-3773(20020703)41:13<2368::AID-ANIE2368>3.0.CO;2-G.

[24] K. Boldt, N. Kirkwood, G.A. Beane, P. Mulvaney, Synthesis of highly luminescent and photo-stable, graded shell CdSe/Cd $_xZn_{1-x}S$ nanoparticles by in situ alloying, Chem. Mater. 25 (2013) 4731–4738. doi:10.1021/cm402645r.

[25] S. Mourdikoudis, L.M. Liz-marza, Oleylamine in Nanoparticle Synthesis Oleylamine in Nanoparticle Synthesis, Chem. Mater. 25 (2016) 1465–1476. doi:10.1021/cm4000476.

[26] X. Peng, J. Thessing, Controlled synthesis of high quality semiconductor nanocrystals, Struct. Bond. 118 (2005) 79–119. doi:10.1007/b137472.

[27] X. Zhong, Y. Feng, W. Knoll, M. Han, Alloyed $Zn_xCd_{1-x}S$ Nanocrystals with Highly Narrow Luminescence Spectral Width, J. Am. Chem. Soc. 125 (2003) 13559–13563. doi:10.1021/ja036683a.

[28] Y.X. Huang, S.R. Chung, Encapsulate Materials Effect on $Zn_xCd_{1-x}S$ White Light Quantum Dots-Based White Light-Emitting Diodes, IOP Conf. Ser. Mater. Sci. Eng. 739 (2020) 1–6. doi:10.1088/1757-899X/739/1/012019.

[29] T.P.A. Ruberu, H.R. Albright, B. Callis, B. Ward, J. Cisneros, H. Fan, J. Vela, Molecular Control of the Nanoscale: Effect of Phosphine–Chalcogenide Reactivity on CdS–CdSe Nanocrystal Composition and Morphology, ACS Nano. 6 (2012) 5348–5359. doi:10.1021/nn301182h.

[30] M.D. Regulacio, M.Y. Han, Composition-tunable alloyed semiconductor nanocrystals, Acc. Chem. Res. 43 (2010) 621–630. doi:10.1021/ar900242r.

[31] L. Loghina, M. Grinco, A. Iakovleva, S. Slang, K. Palka, M. Vlcek, Mechanistic investigation of the sulfur precursor evolution in the synthesis of highly photoluminescent $Cd_{0.15}Zn_{0.85}S$ quantum dots, New J. Chem. 42 (2018) 14779–14788. doi:10.1039/C8NJ03077D.

[32] A. Iakovleva, L. Loghina, Z. Olmrova Zmrhalova, J. Mistrik, P. Svec, S. Slang, K. Palka, M. Vlcek, Environmentally friendly approach to the synthesis of monodisperse and bright blue emitting $Cd_{0.15}Zn_{0.85}S$ quantum dots, J. Alloys Compd. 812 (2020) 152159. doi:10.1016/j.jallcom.2019.152159.

[33] G. Osmond, Zinc Soaps: An Overview of Zinc Oxide Reactivity and Consequences of Soap Formation in Oil-Based Paintings, in: Springer Int. Publ. - Cult. Herit. Sci., 2019: pp. 25–46. doi:10.1007/978-3-319-90617-1_2.

[34] G. Socrates, Infrared and Raman characteristic group frequencies. Tables and charts, 2001. doi:10.1002/jrs.1238.

[35] A. Kaderavkova, L. Loghina, M. Chylii, S. Slang, P. Placek, B. Frumarova, M. Vlcek, N,N',N'-trisubstituted thiourea as a novel sulfur source for the synthesis of Mn-doped ZnS QDs, J. Alloys Compd. 831 (2020) 154814. doi:10.1016/j.jallcom.2020.154814.

[36] I.O. Perez De Berti, M. V. Cagnoli, G. Pecchi, J.L. Alessandrini, S.J. Stewart, J.F. Bengoa, S.G. Marchetti, Alternative low-cost approach to the synthesis of magnetic iron oxide nanoparticles by thermal decomposition of organic precursors, Nanotechnology. 24 (2013). doi:10.1088/0957-4484/24/17/175601.

[37] K. Nakamoto, Infrared and Raman Spectra of Inorganic and Coordination Compounds, John Wiley & Sons, Inc., Hoboken, NJ, USA, 2008. doi:10.1002/9780470405840.

[38] S. Srivastava, Infrared Active Two-Phonon Processes in Cubic ZnS, Aust. J. Phys. 26 (1973) 111. doi:10.1071/PH730111.

[39] C.A. Klein, R.N. Donadio, Infrared-active phonons in cubic zinc sulfide, J. Appl. Phys. 51 (1980) 797–800. doi:10.1063/1.327295.

[40] R. Marshall, S.S. Mitra, Optically active phonon processes in CdS and ZnS, Phys. Rev. 134 (1964). doi:10.1103/PhysRev.134.A1019.

[41] J. Trajić, M. Gilić, N. Romčević, M. Romčević, G. Stanišić, Z. Lazarević, D. Joksimović, I.S. Yahia, Far-infrared investigations of the surface modes in CdS thin films, Phys. Scr. T162 (2014). doi:10.1088/0031-8949/2014/T162/014031.

[42] C.Y. Yeh, Z.W. Lu, S. Froyen, A. Zunger, Zinc-blende - wurtzite polytypism in semiconductors, Phys. Rev. B. 46 (1992) 10086–10097. doi:10.1103/PhysRevB.46.10086.

[43] Z. Jiang, Y. Lei, Z. Zhang, J. Hu, Y. Lin, Z. Ouyang, Nitrogen-doped graphene quantum dots decorated $Zn_xCd_{1-x}S$ semiconductor with tunable photoelectric properties, J. Alloys Compd. 812 (2020) 152096. doi:10.1016/j.jallcom.2019.152096.

[44] I.E. Borissevitch, E.P. Lukashev, I.P. Oleinikov, A.L.S. Pavanelli, P.J. Gonçalves, P.P. Knox, Electrostatic interactions and covalent binding effects on the energy transfer between quantum dots and reaction centers of purple bacteria, J. Lumin. 207 (2019) 129–136. doi:10.1016/j.jlumin.2018.11.013.

[45] Y. Shen, R. Tan, M.Y. Gee, A.B. Greytak, Quantum yield regeneration: Influence of neutral ligand binding on photophysical properties in colloidal core/shell quantum dots, ACS Nano. 9 (2015) 3345–3359. doi:10.1021/acsnano.5b00671.

[46] M.S. Smirnov, O. V. Buganov, S.A. Tikhomirov, O. V. Ovchinnikov, Femtosecond dynamics of photoexcitation in hybrid systems of CdS quantum dots with methylene blue, Phys. E Low-Dimensional Syst. Nanostructures. 118 (2020) 113898. doi:10.1016/j.physe.2019.113898.

[47] C.Q. Wang, J.X. Xia, M.U. Ali, M. Liu, W. Lu, H. Meng, Facile synthesis of enhanced photoluminescent Mg:CdZnS/Mg:ZnS core/shell quantum dots, Mater. Sci. Semicond. Process. 92 (2019) 96–102. doi:10.1016/j.mssp.2018.07.007.

[48] J. Tauc, A. Menth, States in the gap, J. Non. Cryst. Solids. 8–10 (1972) 569–585. doi:10.1016/0022-3093(72)90194-9.

[49] G.A. Reynolds, K.H. Drexhage, New coumarin dyes with rigidized structure for flashlamp-pumped dye lasers, Opt. Commun. 13 (1975) 222–225. doi:10.1016/0030-4018(75)90085-1.

[50] A.P. Gaikwad, D. Tyagi, C.A. Betty, R. Sasikala, Photocatalytic and photo electrochemical properties of cadmium zinc sulfide solid solution in the presence of Pt and RuS_2 dual co-catalysts, Appl. Catal. A Gen. 517 (2016) 91–99. doi:10.1016/j.apcata.2016.03.006.

[51] W.S. Chae, T.D.T. Ung, Q.L. Nguyen, Time-resolved photoluminescence and photostability of single semiconductor quantum dots, Adv. Nat. Sci. Nanosci. Nanotechnol. 4 (2013). doi:10.1088/2043-6262/4/4/045009.

[52] A.J. Wojtowicz, J. Glodo, W. Drozdowski, K.R. Przegietka, Electron traps and scintillation mechanism in $YAlO_3$:Ce and $LuAlO_3$:Ce scintillators, J. Lumin. 79 (1998) 275–291. doi:10.1016/S0022-2313(98)00039-8.

[53] M.D. Garrett, A.D. Dukes III, J.R. McBride, N.J. Smith, S.J. Pennycook, S.J. Rosenthal, Band Edge Recombination in CdSe, CdS and CdS_xSe_{1-x} Alloy Nanocrystals Observed by Ultrafast Fluorescence Upconversion: The Effect of Surface Trap States, J. Phys. Chem. C. 112 (2008) 12736–12746. doi:10.1021/jp803708r.

[54] J. Park, J. Nam, N. Won, H. Jin, S. Jung, S. Jung, S.H. Cho, S. Kim, Compact and stable quantum dots with positive, negative, or zwitterionic surface: Specific cell interactions and non-specific adsorptions by the surface charges, Adv. Funct. Mater. 21 (2011) 1558–1566. doi:10.1002/adfm.201001924.

[55] S. V. Dezhurov, A.Y. Trifonov, M. V. Lovygin, A. V. Rybakova, D. V. Krylsky, Synthesis of highly photostable NIR-emitting quantum dots CdTeSe/CdS/CdZnS/ZnS, Nanotechnologies Russ. 11 (2016) 337–343. doi:10.1134/S199507801603006X.

[56] P.O. Anikeeva, J.E. Halpert, M.G. Bawendi, V. Bulović, Quantum dot light-emitting devices with electroluminescence tunable over the entire visible spectrum, Nano Lett. 9 (2009) 2532–2536. doi:10.1021/nl9002969.

[57] T. Cheng, F. Wang, W. Sun, Z. Wang, J. Zhang, B. You, Y. Li, T. Hayat, A. Alsaed, Z. Tan, High-Performance Blue Quantum Dot Light-Emitting Diodes with Balanced Charge Injection, Adv. Electron. Mater. 5 (2019) 1800794. doi:10.1002/aelm.201800794.